

## 3-bromo-6-nitro-1-(prop-2-yn-1-yl)-1H-indazole as novel corrosion inhibitor for mild steel: Experimental and Quantum Chemical study

M. M. Mohamed Abdelahi<sup>1</sup>, H. Elmsellem<sup>2\*</sup>, N. K. Sebbar<sup>1</sup>, A. Chetouani<sup>2</sup>, L. El Ouasif<sup>1</sup>,  
A. E. Jilalat<sup>1</sup>, E. M. Essassi<sup>1,3</sup>, M. Benchidmi<sup>1</sup>, M. A. Shariati<sup>4</sup>

<sup>1</sup>Laboratoire de Chimie Organique Hétérocyclique, URAC 21, Pôle de Compétences Pharmacochimie, Mohammed V University in Rabat, Faculté des Sciences, Av. Ibn Battouta, BP 1014 Rabat, Morocco.

<sup>2</sup>Laboratoire de chimie analytique appliquée, matériaux et environnement (LC2AME), Faculté des Sciences, B.P. 717, 60000 Oujda, Morocco.

<sup>3</sup>Moroccan Foundation for Advanced Science, Innovation and Research (MASCIR), Rabat Design Center, Rue Mohamed Al Jazouli, Madinat El Irfane, Rabat, Morocco.

<sup>4</sup>Research Department, LLC «Science & Education», and Researcher, All Russian Research Institute of Phytopathology, Moscow Region, Russia.

Received 12 Jan 2017,  
Revised 21 Mar 2017,  
Accepted 25 Mar 2017

### Keywords

- ✓ Indazole;
- ✓ Corrosion;
- ✓ EIS ;
- ✓ Inhibitor;
- ✓ DFT;
- ✓ Fukui function ;
- ✓ MS;

H. Elmsellem

[h.elmsellem@gmail.com](mailto:h.elmsellem@gmail.com)

Phone: (+212)0600254809

### ABSTRACT

Corrosion inhibition performance of 3-bromo-6-nitro-1-(prop-2-yn-1-yl)-1H-indazole (E1) on the corrosion behavior of MS surface in 1.0 M HCl was investigated by gravimetric, analytical methods potentiodynamic polarization and electrochemical impedance spectroscopy and supported by quantum chemical calculation. The inhibition efficiency of E1 was found to increase with increasing inhibitor concentration. The E% reached 87% at 10<sup>-3</sup>M. Polarization studies showed that this compound was cathodic inhibitor. The inhibition actions of this compound were discussed in view of blocking the electrode surface by means of adsorption of inhibitor molecule obeying Langmuir adsorption isotherm. Data obtained for inhibition efficiency from the two test techniques are in reasonably good agreement with quantum chemical parameters calculated at DFT/B3LYB/6-31G (d, p).

## 1. Introduction

Corrosion inhibition of materials has been the focus of research for centuries and in many cases has been well analyzed and understood [1-4]. Corrosion of materials has continued to receive interest in the technological world. In the field of corrosion inhibition, scientists are persistent in seeking better and more efficient ways of combating the corrosion of metals. Addition of corrosion inhibitors to the corrosion environment with respect to the other methods of corrosion inhibition has been employed [5]. The use of inhibitors is one of the most practical methods for protection against corrosion in acidic media. To be effective, an inhibitor must also transfer water from the metal surface, interact with anodic or cathodic reaction sites to retard the oxidation and reduction corrosion reaction, and prevent transportation of water and corrosion-active species on the metal surface. Mild steel is one of the most frequently used materials in many engineering applications like parts of machines, pipelines, boilers and in chemical storage. It has natural tendency to corrode whenever it comes in contact with corrosive or reactive environments [6-8]. Normally metals corrode at slow rate in air but when acid interacts with the metals, corrosion rate becomes very high [9-10]. Several methods are used to protect metals and alloys from corrosion but the use of inhibitors to protect the metals in the corrosive environment is one of the most common methods. Organic compounds which have different heteroatoms such as N, O, S, P, and aromatic rings in their structure are reported as effective inhibitors [11-14].

Indazole derivatives have been extensively studied because of their interesting chemical and pharmacological activities [15] including antitumor [16], antiplatelet [17], anti-viral [18], anti-microbial [19], anti-cataract [20], anti-cancer [21], anti-inflammatory [22], antimicrobial [23] and anti-spermatogenic [24].

The adsorption ability of inhibitors onto metal surface depends on the nature and surface charge of metal, the chemical composition of electrolytes, and the molecular structure and electronic characteristics of inhibitor molecules. Density functional theory (DFT) has grown to be an useful theoretical method to interpret experimental results, enabling one to obtain structural parameters for even huge complex molecules, and it can explain the hard and soft acid base (HSAB) behavior of organic molecules. DFT connects some traditional empirical concepts with quantum mechanical interpretations [25, 26]. Therefore, DFT is a very powerful technique to probe the inhibitor/surface interaction and to analyze experimental data. In this work, the efficacy of the organic compound 3-bromo-6-nitro-1-(prop-2-yn-1-yl)-1H-indazole (E1) (**Figure 1**) as corrosion inhibitor for mild steel in 1 M HCl solution using electrochemical techniques. Thermodynamic activation parameters were evaluated from experimental data. The relationships between the inhibition performances of the investigated inhibitor in 1M HCl and some quantum chemical parameters, such as the highest occupied molecular orbital energy ( $E_{\text{HOMO}}$ ), the lowest unoccupied molecular orbital energy ( $E_{\text{LUMO}}$ ), the energy gap between  $E_{\text{LUMO}}$  and  $E_{\text{HOMO}}$  ( $\Delta E_{\text{LUMO-HOMO}}$ ) and dipole moments. The molecular structure of (E1) is given in **Figure 1**.

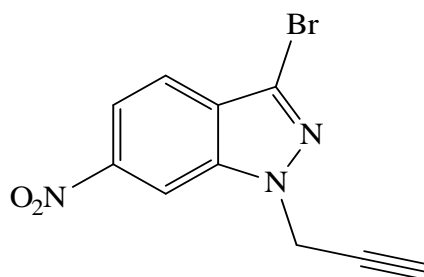
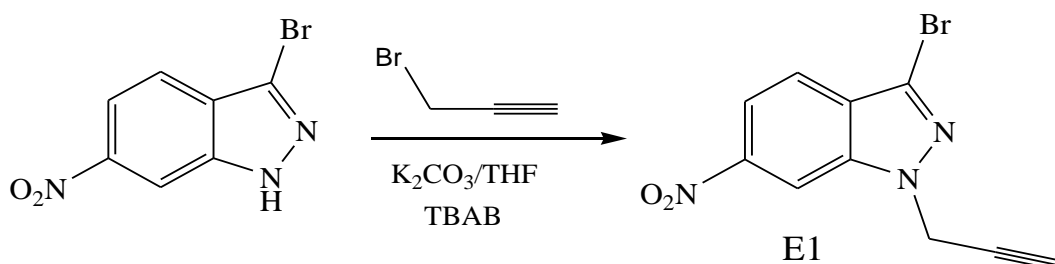


**Figure 1.** Chemical structure of 3-bromo-6-nitro-1-(prop-2-yn-1-yl)-1H-indazole (E1).

## 2. Experimental

### 2.1. Synthesis of inhibitor

To a solution of 0.01 mol (0.5 g) of 3-bromo-6-nitroindazole and 0.01mol (1.2 ml) of propargyl bromide in 40 ml of THF were added 0.01 mol of potassium bicarbonate (1.38 g) and 0.16 g of tetra n-butylammonium bromide (TBAB). The mixture reaction was stirred for 48 h after that THF was removed under vacuum. The final product was purified by chromatography on silica gel with hexane/ ethyl acetate (8:2) as eluent, and recrystallized from ethanol ethanol.



**Scheme 1.** Synthesis of 3-bromo-6-nitro-1-(prop-2-yn-1-yl)-1H-indazole (E1).

Yield: 78%; mp: 505K;  $^1\text{H NMR}$  (300 MHz, DMSO- $d_6$ )  $\delta$  (ppm): 3.51(t,  $J=2.55\text{Hz}$ , 2H); 5.56 (d,  $J=2.55\text{Hz}$ , 2 H); 7.85 (dd,  $J=0.6\text{Hz}$ ,  $J=9\text{Hz}$ , 1H); 8.05 (dd,  $J=1.8\text{Hz}$ ,  $J=9\text{Hz}$ , 1H ) 8.89 (dd,  $J=0.6\text{Hz}$ ,  $J=1.8\text{Hz}$ , 1H).  $^{13}\text{C NMR}$  (75 MHz, DMSO- $d_6$ )  $\delta$ (ppm): 39.70 (CH<sub>2</sub>); 77.5 (CH); 78.35 (Cq); 108.07-117.02-121.33 (CH, Ar) 126.68 (Cq-Br); 121.83 -139.51-147.70 (Cq, Ar) (**Figure 2**).

### 2.2. Theory and computational details

Quantum chemical calculations are used to correlate experimental data for inhibitors obtained from different techniques (viz., electrochemical and weight loss) and their structural and electronic properties. According to Koop man's theorem [27],  $E_{\text{HOMO}}$  and  $E_{\text{LUMO}}$  of the inhibitor molecule are related to the ionization potential (I) and the electron affinity (A), respectively. The ionization potential and the electron affinity are defined as  $I = -E_{\text{HOMO}}$  and  $A = -E_{\text{LUMO}}$ , respectively.

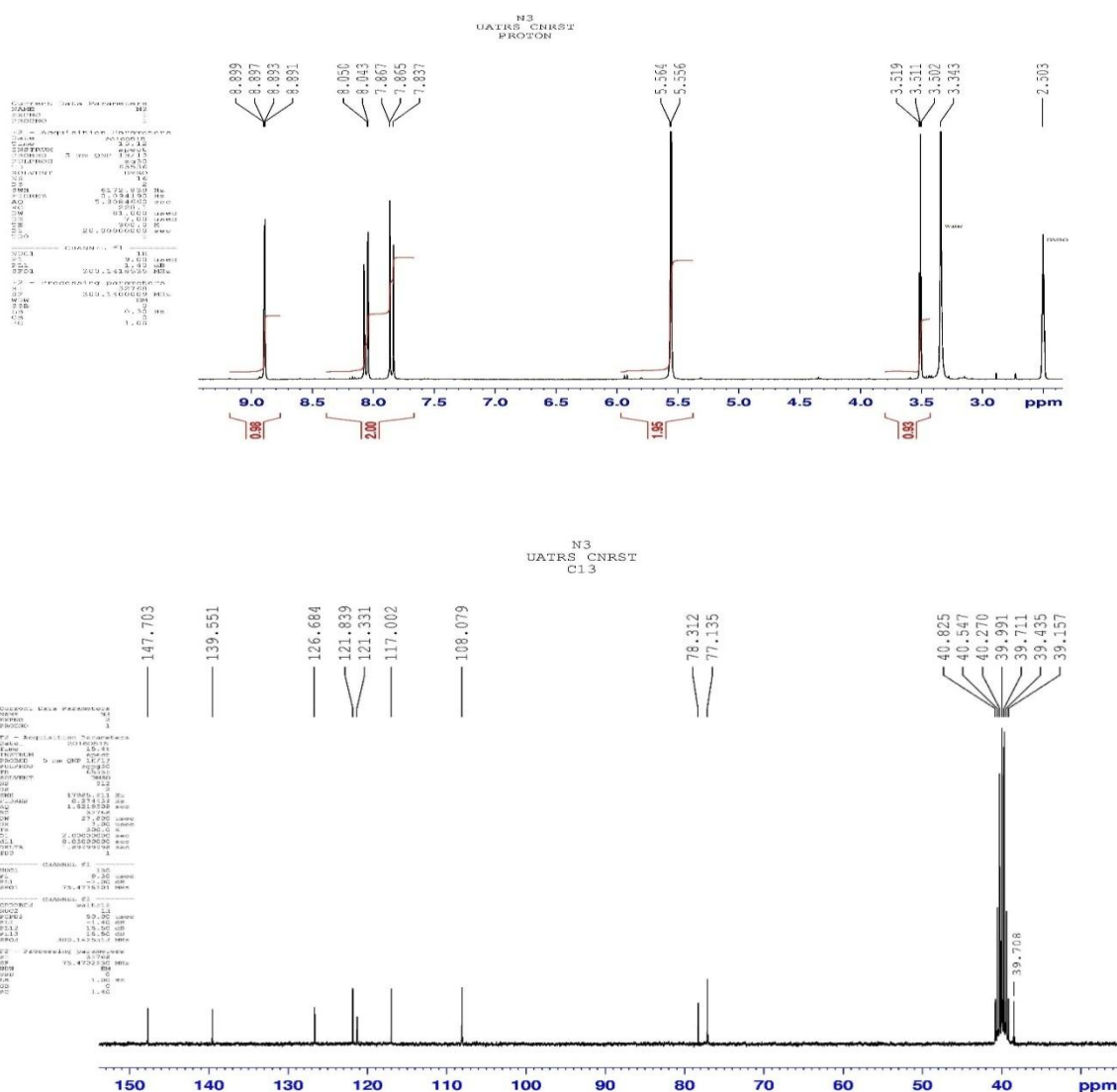


**Figure 2:**  $^1\text{H}$  NMR and  $^{13}\text{C}$  NMR spectrum of (E1).

Then absolute electronegativity ( $\chi$ ) and global hardness ( $\eta$ ) of the inhibitor molecule are approximated as follows [28]:

$$\chi = \frac{I+A}{2}, \quad \chi = -\frac{1}{2}(E_{HOMO} + E_{LUMO}) \quad (1)$$

$$\eta = \frac{I-A}{2}, \quad \eta = -\frac{1}{2}(E_{HOMO} - E_{LUMO}) \quad (2)$$

Where  $I = -E_{HOMO}$  and  $A = -E_{LUMO}$  are the ionization potential and electron affinity respectively.

The fraction of transferred electrons  $\Delta N$  was calculated according to Pearson theory [27]. This parameter evaluates the electronic flow in a reaction of two systems with different electronegativities, in particular case; a metallic surface (Fe) and an inhibitor molecule.  $\Delta N$  is given as follows:

$$\Delta N = \frac{\chi_{Fe} - \chi_{inh}}{2(\eta_{Fe} + \eta_{inh})} \quad (3)$$

Where  $\chi_{Fe}$  and  $\chi_{inh}$  denote the absolute electronegativity of an iron atom (Fe) and the inhibitor molecule, respectively;  $\eta_{Fe}$  and  $\eta_{inh}$  denote the absolute hardness of Fe atom and the inhibitor molecule, respectively. In order to apply the eq.4 in the present study, a theoretical value for the electronegativity of bulk iron was used  $\chi_{Fe} = 7$  eV and a global hardness of  $\eta_{Fe} = 0$ , by assuming that for a metallic bulk  $I = A$  because they are softer than the neutral metallic atoms [29].

The electrophilicity has been introduced by Sastri and al. [28], is a descriptor of reactivity that allows a quantitative classification of the global electrophilic nature of a compound within a relative scale. They have proposed the  $\omega$  as a measure of energy lowering owing to maximal electron flow between donor and acceptor and  $\omega$  is defined as follows:

$$\omega = \frac{\chi^2}{2\eta} \quad (4)$$

The Softness  $\sigma$  is defined as the inverse of the  $\eta$  [30]:

$$\sigma = \frac{1}{\eta} \quad (5)$$

Using left and right derivatives with respect to the number of electrons, electrophilic and nucleophilic Fukui functions for a site  $k$  in a molecule can be defined [30]:

$$f_k^+ = P_k(N + 1) - P_k(N) \quad \text{for nucleophilic attack} \quad (6)$$

$$f_k^- = P_k(N) - P_k(N - 1) \quad \text{for electrophilic attack} \quad (7)$$

$$f_k^{\cdot} = [P_k(N + 1) - P_k(N - 1)]/2 \quad \text{for radical attack} \quad (8)$$

### 3. Results and discussion

#### 3.1. Gravimetric measurements

The corrosion rate of MS specimens after exposure to 1M HCl solution with and without the addition of various concentrations of 3-bromo-6-nitro-1-(prop-2-yn-1-yl)-1H-indazole (E1) was calculated in  $\text{mg cm}^{-2} \text{h}^{-1}$  and the data obtained are given in Table 1.

The inhibition efficiencies ( $E_w\%$ ) were calculated and the data obtained given in the same Table 1. It can be seen from Table 1 that, the addition of E1 to the aggressive solution reduces the corrosion rate of MS. The corrosion rate decreased and inhibition efficiency increased with increasing inhibitor concentration suggests that the inhibitor molecules act by adsorption on the metal surface [31].

The corrosion behavior of MS in 1 M HCl in the absence and presence of E1 was studied at temperature 308K using weight loss technique and data obtained at time (6h) are shown in Table 1.

The corrosion rate ( $v$ ) is calculated using the following equation:

$$v = \frac{w}{st} \quad (9)$$

Where:  $w$  is the average weight loss,  $S$  the total area, and  $t$  is immersion time. With the corrosion rate calculated, the inhibition efficiency ( $E_w$ ) is determined as follows:

$$E_w \% = \frac{v_0 - v}{v_0} \times 100 \quad (10)$$

Where:  $v_0$  and  $v$  are, respectively, the values of corrosion rate with and without inhibitor.

**Table 1:** Weight loss values of various concentrations of E1 in 1M HCl solution at 308 K

Inhibitor	Concentration (M)	$v$ ( $\text{mg.cm}^{-2} \text{h}^{-1}$ )	$E_w$ (%)	$\theta$
1M HCl	--	0.828	--	--
3-bromo-6-nitro-1-(prop-2-yn-1-yl)-1H-indazole E1	$10^{-6}$	0.345	58	0.58
	$10^{-5}$	0.288	65	0.65
	$10^{-4}$	0.192	77	0.77
	$10^{-3}$	0.113	86	0.86

#### 3.2. Adsorption isotherm

The adsorption isotherm that describes the adsorptive behavior of organic inhibitors is important in order to know the mechanism of corrosion inhibition. Basic information dealing with interaction between the inhibitor

molecules and the metal surface can be provided by adsorption isotherms. Several adsorption isotherms were attempted to fit the degree of surface coverage values ( $\theta$ ) to adsorption isotherms including Frumkin, Temkin, Freundlich and Langmuir isotherms. The  $\theta$  values for various concentrations of inhibitor in acidic media have been evaluated from the gravimetric measurements (Table 2). The best fit was obtained in the case of Langmuir isotherm which assumes that the solid surface contains a fixed number of adsorption sites and each site holds one adsorbed species [31]. The plot of  $C_{inh}/\theta$  vs.  $C_{inh}$  (Figure3) yields a straight line with correlation coefficient of 0.999 for both mediums providing that the adsorption of E1 on the MS surface obeys Langmuir adsorption isotherm. This isotherm can be represented as [32]:

$$\frac{C}{\theta} = \frac{1}{K} + C \quad (11)$$

Where  $C_{inh}$  is the molar concentration of the inhibitor and  $K_{ads}$  is the equilibrium constant for the adsorption-desorption process. The value of  $K_{ads}$  (Figure3) was found to be  $1.63 \times 10^5 \text{ M}^{-1}$  in 1.0 M HCl.

The relatively high value of adsorption equilibrium constant reflects the high adsorption ability of E1 on MS surface [32]. The  $K_{ads}$  is related to the standard free energy of adsorption, by the following equation[33]:

$$\Delta G_{ads} = -RT \cdot \ln(55.5 \cdot K) \quad (12)$$

Where R is gas constant and T is absolute temperature of experiment and the constant value of 55.5 is the concentration of water in solution in  $\text{mol L}^{-1}$ .

The value was calculated as  $-40.99 \text{ kJ mol}^{-1}$  in 1.0 M HCl. The negative value of indicates the spontaneity of the adsorption process and the stability of adsorbed layer on the MS surface. It is well known that the values of the order of  $-20 \text{ kJ mol}^{-1}$  or lower indicate a physisorption; those of order of  $-40 \text{ kJ mol}^{-1}$  or higher involve charge sharing or transfer from the inhibitor molecules to the metal surface to form a coordinate type of bond (chemisorption) [34]. On the other hand, the adsorption phenomenon of an organic molecule is not considered only as a purely physical or chemical adsorption phenomenon. A wide spectrum of conditions, ranging from the dominance of chemisorption or electrostatic effects, arises from other adsorptions experimental data [34].

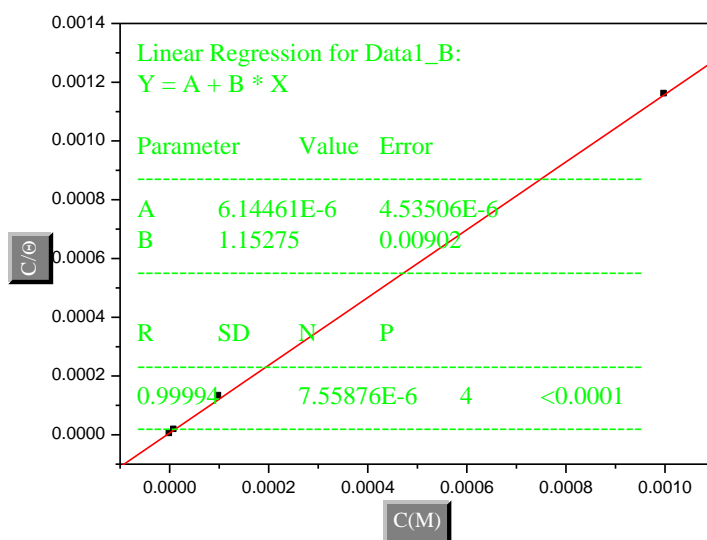


**Figure 3:** Langmuir isotherm of MS in the 1M HCl in presence E1 calculated by weight loss technique at 308.

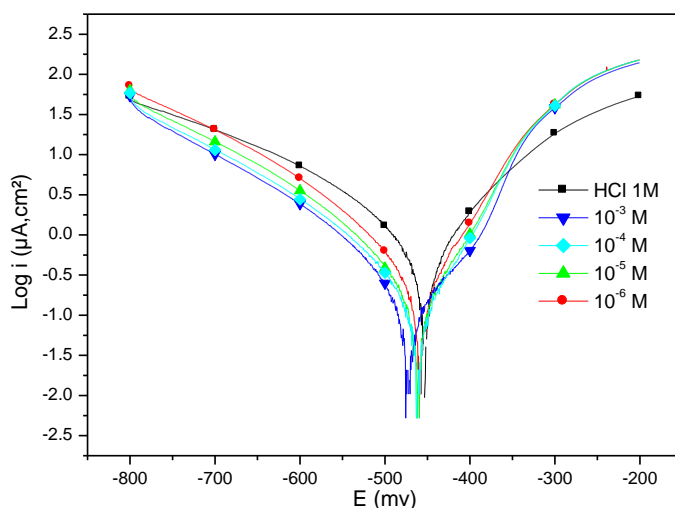
### 3.3. Electrochemical Measurements

The electrochemical measurements were carried out using Volta lab (Tacussel - Radiometer PGZ 100) potentiostat controlled by Tacussel corrosion analysis software model (Voltmaster 4) at static condition. The corrosion cell used had three electrodes. The reference electrode was a saturated calomel electrode (SCE). A platinum electrode was used as auxiliary electrode of surface area of  $1 \text{ cm}^2$ . The working electrode was carbon steel of the surface  $1 \text{ cm}^2$ . All potentials given in this study were referred to this reference electrode. The working electrode was immersed in the test solution for 30 minutes to establish a steady state open circuit potential ( $E_{ocp}$ ). After measuring the  $E_{ocp}$ , the electrochemical measurements were performed. All electrochemical tests have been performed in aerated solutions at 308 K. The EIS experiments were conducted in the frequency range with high limit of 100 kHz and different low limit 0.1 Hz at open circuit potential, with

10 points per decade, at the rest potential, after 30 min of acid immersion, by applying 10 mV ac voltage peak-to-peak. Nyquist plots were made from these experiments. The best semicircle can be fit through the data points in the Nyquist plot using a non-linear least square fit so as to give the intersections with the x-axis.

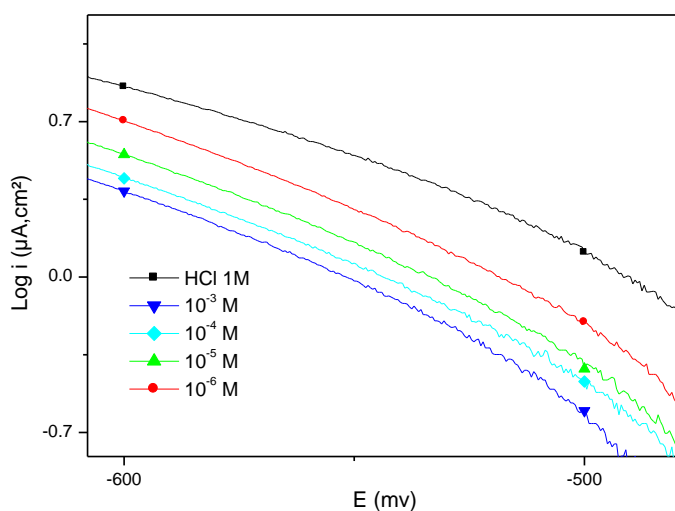
### 3.3.1. Tafel Polarization Study

Figure 4 shows anodic and cathodic polarization plots recorded on MS electrode in 1 M HCl in absence and presence of different concentrations of E1 inhibitor. Electrochemical corrosion parameters, such as corrosion potential  $E_{\text{corr}}$  (mV/SCE), cathodic  $\beta_c$  Tafel slope (mV/dec), the corrosion current density  $I_{\text{corr}}$  ( $\mu\text{A cm}^{-2}$ ) and inhibition efficiency  $E_p$  (%) are given in Table 2.



**Figure 4:** Polarization curves of MS in 1.0 M HCl without and with different concentrations of E1 at 308 K.

From the Figure4, it can be seen that the addition of E1 causes a remarkable decrease in the corrosion rate i.e., shifts the cathodic curves to lower current densities. In other words, both cathodic and anodic reactions of MS electrode are drastically inhibited after the addition of E1. This may be ascribed to adsorption of inhibitor over the corroded surface of MS[35]. The cathodic current–potential curves (Figure5) give rise to parallel lines indicating that the addition of E1 to the 1M HCl solutions does not modify the hydrogen evolution mechanism and the reduction of  $\text{H}^+$  ions at the MS surface which occurs mainly through a charge transfer mechanism. The inhibitor molecules are first adsorbed onto MS surface and blocking the available reaction sites. In this way, the surface area available for  $\text{H}^+$  ions decreases while the actual reaction mechanism remains unaffected [36].



**Figure 5:** The cathodic parallel lines (curve current–potential).

**Table 2.** Electrochemical parameters and corresponding inhibition efficiency for corrosion of the MS in 1.0 M HCl in the absence and the presence of different concentrations of E1 at 308 K.

	Concentration (M)	$E_{corr}$ (mV/SCE)	$-\beta_c$ (mV/dec)	$I_{corr}$ (mA/cm <sup>2</sup> )	E (%)
1M HCl	--	-454	140	1381	--
E1	$10^{-3}$	-461	136	689	50
	$10^{-4}$	-473	123	465	66
	$10^{-5}$	-461	119	352	75
	$10^{-6}$	-459	104	251	82

From Table 2, also can find that the corrosion potentials of inhibitor shift slightly in the positive direction in HCl to negative direction. On the other hand, in both mediums, the cathodic Tafel slope  $\beta_c$  change with insignificant trend in anodic and cathodic directions. From previous results, it can be concluded that tested inhibitor probably act as cathodic inhibitor in HCl [37]. As it can be seen from Table 2, in both solutions when the concentration of inhibitor increases the inhibition efficiencies increase, while corrosion current densities decrease. The results obtained in both mediums by potentiodynamic polarization confirm the better inhibitive performance of investigated inhibitor.

### 3.3.2. Electrochemical impedance spectroscopy (EIS)

In order to better define the effect of our additive and concentration on the corrosion process, Nyquist plots of MS in uninhibited and inhibited acidic solutions containing various concentrations of 3-bromo-6-nitro-1-(prop-2-yn-1-yl)-1H-indazole (E1) are shown in Figure6 in 1.0 M HCl.

The existence of a single semicircle shows a single charge transfer process during dissolution which is unaffected by the presence of inhibitor molecules. Deviations from perfect circular shape are often referred to the frequency dispersion of interfacial impedance, which arises due to surface roughness, impurities, dislocations, grain boundaries, adsorption of inhibitor, and formation of porous layers and in homogenates of the electrode surface [37-38].

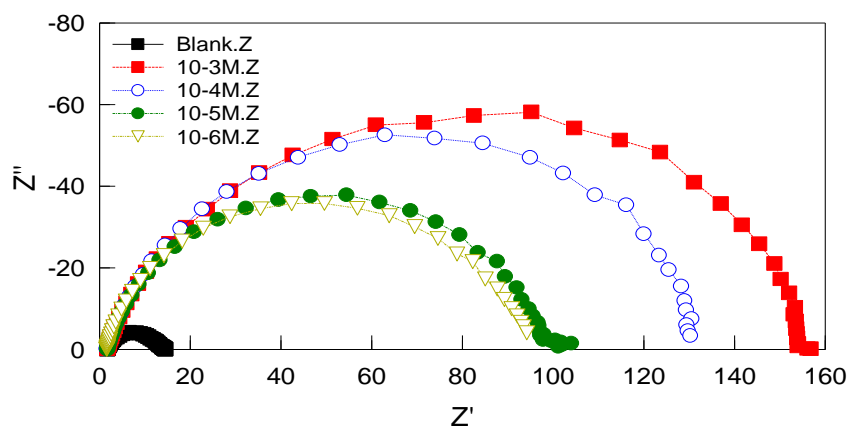


**Figure 6:** Nyquist plots of MS in 1.0M HCl without and with different concentrations of E1 at 308k.

The diameter of the semicircle increases after the addition of E1 to the aggressive solution. This increase more and more pronounced with increasing inhibitor E1 concentration. The electrochemical parameters derived from EIS measurements (including,  $R_{ct}$ , transfer charge, double layer capacitance  $C_{dl}$  ( $\mu\text{F cm}^{-2}$ ) and the inhibitor efficiency values  $E$  (%) are given in Table 3. Double layer capacitance values were obtained at maximum frequency ( $f_{max}$ ) at which the imaginary component of the Nyquist plot is maximum and calculated using the following equation [39]:

It is evident from the results collected in Table 3, that E1 inhibits the corrosion of MS in 1 M HCl at all the concentrations used, and the inhibition efficiency ( $E\%$ ) increases continuously with increasing concentrations at 308K. EIS results show also that the  $R_{ct}$  values increase and the  $C_{dl}$  values decrease with increasing the inhibitor concentration. The increase in  $R_{ct}$  value can be attributed to the formation of protective film on the

metal/solution interface [40]. On the other hand, the decrease in Cdl values can result from a decrease in local dielectric constant and/or an increase in the thickness of the electrical double layer. It can be assumed that the decrease of Cdl values is caused by the gradual replacement of water molecules by adsorption of inhibitor molecules on the MS surface [41].

**Table 3.** Electrochemical impedance parameters and inhibition efficiency for MS in 1.0 M HCl solution with E1 at 308K.

Concentration (M) \ Parameters	1M HCl	10 <sup>-6</sup>	10 <sup>-5</sup>	10 <sup>-4</sup>	10 <sup>-3</sup>
Real Center	9.25	47.96	50.01	67.31	79.22
Imag. Center	1.62	12.12	12.06	14.77	22.47
Diameter	15.13	96.24	99.72	134.19	161.06
n	0.81	0.71	0.82	0.87	0.79
Low Intercept R <sub>s</sub> (Ω.cm <sup>2</sup> )	1.86	1.39	1.63	1.86	1.89
High Intercept R <sub>t</sub> (Ω.cm <sup>2</sup> )	16.64	94.536	98.393	132.77	156.56
Depression Angle	12.42	14.58	14.00	12.71	16.20
ω <sub>max</sub> (rad s <sup>-1</sup> )	929.60	184.69	113.41	89.66	66.8
Estimated R <sub>t</sub> (Ω.cm <sup>2</sup> )	14.78	93.14	96.75	130.90	154.66
Estimated C <sub>dl</sub> (F.cm <sup>-2</sup> )	7.11 E-5	6.45E-5	5.84E-5	4.31E-5	3.29E-5
E (%)	--	83	85	88	<b>90</b>

EIS spectra of the E1 were analyzed using the equivalent circuit which is shown in Figure 7. indicates that a single charge transfer reaction and fits well with our experimental results. The constant phase element, CPE, is introduced in the circuit instead of a pure double layer capacitor to give a more accurate fit [42].

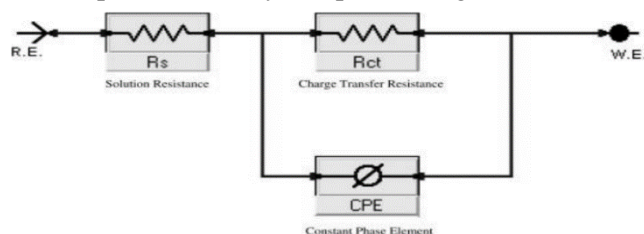


**Figure 7:** Equivalent circuit model used to fit experimental EIS.

### 3.4. Quantum chemical calculations

The chemical reactivity can be explained according to the frontier molecular orbital theory, by the interaction between the HOMO (the highest occupied molecular orbital) and LUMO (lowest unoccupied molecular orbital) of the reacting species. All the global chemical indexes are summarized in Table 4. The FMOs (HOMO and LUMO) are very important for describing chemical reactivity. The HOMO containing electrons, represents the ability ( $E_{\text{HOMO}}$ ) to donate an electron, whereas, LUMO haven't not electrons, as an electron acceptor represents the ability ( $E_{\text{LUMO}}$ ) to obtain an electron. The energy gap between HOMO and LUMO determines the kinetic stability, chemical reactivity, optical polarizability and chemical hardness–softness of a compound [43]. Firstly, in this study, we calculated the HOMO and LUMO orbital energies by using B3LYP method with 6-31G(d,p). All other calculations were performed using the results with some assumptions. The higher values of  $E_{\text{HOMO}}$  indicate an increase for the electron donor and this means a better inhibitory activity with increasing adsorption of the inhibitor on a metal surface, where as  $E_{\text{LUMO}}$  indicates the ability to accept electron of the molecule. The adsorption ability of the inhibitor to the metal surface increases with increasing of  $E_{\text{HOMO}}$  and decreasing of  $E_{\text{LUMO}}$ . The HOMO and LUMO orbital energies and image of P1 were performed and were shown in Table 4 and Figure 8. High ionization energy ( $I = 6.9130$  eV,  $I = 6.7916$  eV in gas and aqueous phases respectively)

indicates high stability [44], the number of electrons transferred ( $\Delta N$ ) was also calculated and tabulated in Table 1. The  $\Delta N < 3.6$  indicates the tendency of a molecule to donate electrons to the metal surface [45-46].

**Table 4.** Quantum chemical descriptors of the studied inhibitors at B3LYP/6-31 G\*\* in gas, G and aqueous, A phases and the inhibition efficiencies as given in [47, 48].

Inhibitor	Phase	$TE$ (eV)	$E_{HOMO}$ (eV)	$E_{LUMO}$ (eV)	Gap $\Delta E$ (eV)	$\mu$ (D)	IP (eV)	EA (eV)	$X$ (eV)	$\eta$ (eV)	$\omega$	$\sigma$	$\Delta N$
E1	G	-31540.3	-6.9130	-3.1751	3.7378	2.6726	6.9130	3.1751	5.0441	1.8689	6.8067	0.5351	0.5233
	A	-31540.6	-6.7916	-3.3044	3.4872	3.0180	6.7916	3.3044	5.0480	1.7436	7.3073	0.5735	0.5598

To get some insight into the local reactivity of the studied inhibitors, the Fukui functions were computed since they are the relevant reactivity indicators in the electron-transfer controlled reactions such as corrosion inhibition process [49, 50]. Their values are used to identify which atoms in the inhibitors are more prone to undergo an electrophilic or a nucleophilic attack.

For a system of  $N$  electrons, independent single-point calculations were made for corresponding  $N+1$  and  $N-1$  electron systems. The resulting natural population analysis yields to  $P_k(N-1)$ ,  $P_k(N)$ , and  $P_k(N+1)$ , the population for all atoms  $k$ . In a finite-difference approximation from Mulliken population analysis of atoms in molecules, depending on the direction of the electron transfer, then the condensed Fukui functions were computed using the following equations from the Exact Theory [50].

The calculated values of the  $f_k^+$  for all inhibitors are mostly localized on the indazole ring. Namely  $C_2$ ,  $Cl_{13}$ ,  $O_{14}$ ,  $O_{15}$ ,  $N_{16}$  and  $C_{21}$ , indicating that the benzodiazepine rings will probably be the favorite site for nucleophilic attacks [51-52]. The results also show that  $O_{15}$  atom is suitable site to undergo both nucleophilic and electrophilic attacks, probably allowing them to adsorb easily and strongly on the MS surface.

**Table 5:** Pertinent natural populations and Fukui functions of E1 calculated at B3LYP/6-31G in gaseous (G) and aqueous phases.

Atom $k$	Phase	$P(N)$	$P(N+1)$	$P(N-1)$	$f_k^-$	$f_k^+$	$f_k^0$
$C_2$	G	0,1851	0,3691	0,3673	0,1840	-0,1822	0,0009
	A	0,3718	0,3841	0,3634	0,0123	0,0084	0,0104
$Cl_{13}$	G	0,2214	0,3838	0,0716	0,1624	0,1498	0,1561
	A	0,1655	0,3323	0,1425	0,1668	0,0230	0,0949
$O_{14}$	G	-0,2041	-0,2303	-0,4551	-0,0262	0,2510	0,1124
	A	-0,3175	-0,2838	-0,5147	0,0337	0,1972	0,1155
$O_{15}$	G	-0,2075	-0,2358	-0,4545	-0,0283	0,2470	0,1094
	A	-0,3169	-0,2819	-0,5111	0,0350	0,1942	0,1146
$N_{16}$	G	-0,3959	-0,5417	-0,611	-0,1458	0,2151	0,0347
	A	-0,6016	-0,5277	-0,6096	0,0739	0,0080	0,0410
$C_{21}$	G	-0,4795	-0,3241	-0,438	0,1554	-0,0415	0,0570
	A	-0,4227	-0,3772	-0,4387	0,0455	0,0160	0,0308

The geometry of E1 in gaseous and aqueous phases (**Figure 8**) was fully optimized using DFT based on Beck's three parameters exchange functional and Lee–Yang–Parr nonlocal correlation functional (B3LYP)[53-54] and the 6–31G. The optimized molecular and selected angles, dihedral angles and bond lengths of E1 are given in (**Figure 8**). The optimized structure shows that the molecule E1 and have a non-planar structure. The HOMO and LUMO electrons density distributions of E1 are given in (**Table 6**).

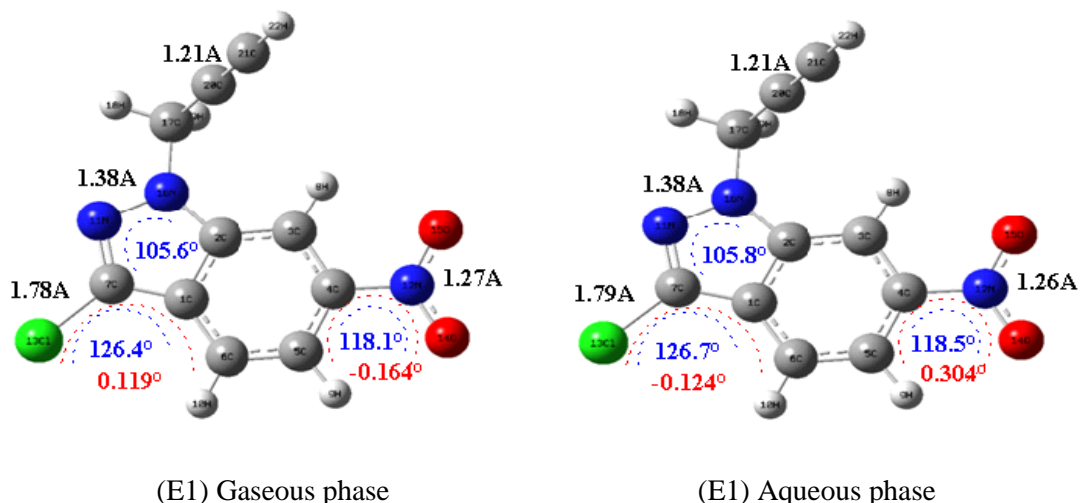


**Figure 8:** Optimized molecular structures and selected dihedral angles (red), angles (blue) and bond lengths (black) of the studied inhibitors calculated in gaseous and aqueous phases using the DFT at the B3LYP/6-31G level.

**Table 6:** The HOMO and the LUMO electrons density distributions of E1 in gaseous and aqueous phases computed at B3LYP/6-31G level for neutral forms.

Inhibitor	Type of MO	Gaseous Phase	Aqueous Phase
E1	HOMO		
	LUMO		

After the analysis of the theoretical results, we can say that the molecule E1 have a non-planar structure. In fact, the CH<sub>2</sub> group is almost perpendicular to the indazole core.

### 3.5. SEM studies

The surface morphology of MS was investigated with scanning electron microscopy (SEM). For this purpose, MS coupons were immersed in blank and 10<sup>-3</sup>M-E1 containing solution, for 6h. After 6h, the coupons removed from the solution, washed with distilled water and dried at room temperature. Then SEM images were taken with 500x magnitudes.

SEM images of MS were obtained in blank and  $10^{-3}$ M-E1 added test solution after 6 h immersion time, given in Figure 9.

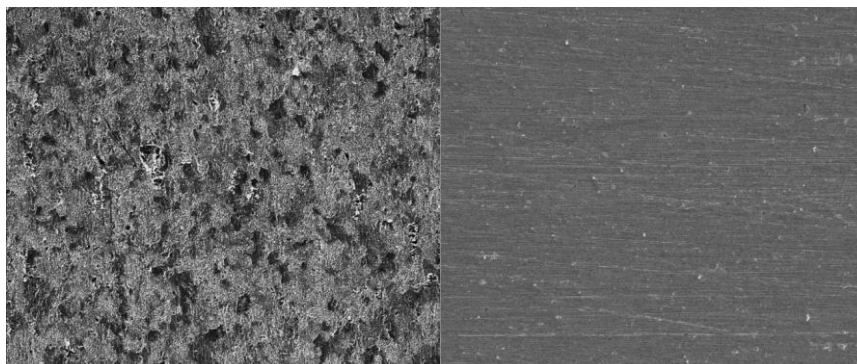


**Figure 9.** SEM images of mild steel coupons after 6 h immersion time in **(left)** 1 M HCl solution; **(right)** with the addition of  $10^{-3}$  M-E1 (The images show x500 magnification).

As can be seen from Figure 9, 6 h immersion time was sufficient to understand the effect of both corrosive environment and inhibitor on MS. The steel surface is highly corroded in HCl solution, due to crystallographic diversities from side to side, there seen some regions more severely damaged than the neighborhood. On the other hand, when inhibitor is added to the corrosive test solution, inhibitor molecules adsorbed on the MS surface strongly, thus a protective layer formed on the MS surface by the  $10^{-3}$ M-E1. The mild steel surface is protected against the attack of corrosive environment by this adsorption layer and corrosion rate is significantly reduced, in 1 M HCl solution in the presence of  $10^{-3}$ M-E1. To sum up, the SEM images together with other results clearly confirmed that protection efficiency of this inhibitor is exceptionally good.

#### 4. Conclusion

According to experimental and theoretical findings, it could be concluded that:

- 3-bromo-6-nitro-1-(prop-2-yn-1-yl)-1H-indazole (E1) is a good corrosion inhibitor for the MS protection in both acid solutions. The inhibitory efficiency of this compound depends on its concentration in both acid solutions.
- EIS plots indicated that  $R_{ct}$  values increase and  $C_{dl}$  values decrease with increasing inhibitor concentration.
- Polarization curves indicated that E1 act as cathodic type inhibitor.
- The adsorption of E1 on the MS surface from two acid solutions follows Langmuir adsorption isotherm. The thermodynamic parameters suggest that this inhibitor E1 is strongly adsorbed on the MS surface.
- The quantum chemical parameters are obtained and discussed in view of experimental results;

#### References

1. Chadli R., Elazouzi M., Khelladi I., Elhourri A.M., Elmsellem H., Aouniti A., Kajima Mulengi J., Hammouti B., *Portugaliae Electrochimica Acta*. 35 (2017) 65-80.
2. Al Mamari K., Elmsellem H., Sebbar K., Elyoussfi A., Steli H., Ellouz M., Ouzidan Y., Nadeem A., Essassi E. M., El-Hajjaji F., *J. Mater. Environ. Sci.* 7 (9) (2016) 3286-3299
3. Elmsellem H., Harit T., Aouniti A., Malek F., Riahi A., Chetouani A., and Hammouti B., *Protection of Metals and Physical Chemistry of Surfaces*. 51 (2015) 873–884.
4. Elmsellem H., Aouniti A., Toubi Y., Steli H., Elazzouzi M., Radi S., Elmahi B., El Ouadi Y., Chetouani A., Hammouti B., *Der Pharma Chemica*. 7(7) (2015) 353-364.
5. Lebrini M., Bentiss F., Vezin H., Lagrene M., *Corros. Sci.* 8 (2006) 1279–1291.
6. Saidi N., Elmsellem H., Ramdani M., Chetouani A., Azzaoui K., Yousfi F., Aouniti A. and Hammouti B., *Der pharma chem.* 7 (2015) 87-94.
7. Elyoussfi A., Dafali A., Elmsellem H., Steli H., Bouzian Y., Cherrak K., El Ouadi Y., Zarrouk A., Hammouti B., *J. Mater. Environ. Sci.* 7 (9) (2016) 3344.
8. Aouniti A., Elmsellem H., Tighadouini S., Elazzouzi M., Radi S., Chetouani A., Hammouti B., Zarrouk A., *J. Taibah Univ. Sci.* 10 (2016) 774-785.

9. Tribak Z., Kandri Rodi Y., Elmsellem H., Abdel-Rahman I., Haoudi A., Skalli M. K., Kadmi Y., Hammouti B., Ali Shariati M., Essassi E. M., *J. Mater. Environ. Sci.* 8 (2017) 1116-1127
10. Benabdellah M., Aouniti A., Dafali A., Hammouti B., Benkaddour M., Yahyi A., Ettouhami A., *Appl. Surf. Sci.* 252 (2006) 8341-8347.
11. Elmsellem H., Aouniti A., Youssoufi M.H., Bendaha H., Ben hadda T., Chetouani A., Warad I., Hammouti B., *Phys. Chem. News.* 70 (2013) 84.
12. Elmsellem H., Basbas N., Chetouani A., Aouniti A., Radi S., Messali M., Hammouti B., *Portugaliae. Electrochimica. Acta.* 2 (2014) 77.
13. Elmsellem H., Bendaha H., Aouniti A., Chetouani A., Mimouni M., Bouyanzer A., *Mor. J. Chem.* 2 (2014) 1.
14. Bendaha H., Elmsellem H., Aouniti A., Mimouni M., Chetouani A., Hammouti B., *Physicochemical Mechanics of Materials.* 1 (2016) 111-118.
15. Lien J.C., Lee F.Y., Huang L.J., Pan S.L., Guh J.H., Teng C.M., Kuo S.C., *J. Med. Chem.* 45 (2002) 4947.
16. Abbassi N., Rakib E. M., Chicha H., Bouissane L., Hannioui A., Aiello C., Gangemi R., Castagnola P., *Archiv der Pharmazie.* 347(6) (2014) 423-431.
17. Selwood D. L., Brummell D. G., Budworth J., Burtin G. E., Campbell R. O., Chana S. S., Charles I. G., Fernandez P. A., Glen R. C., Goggin M. C., Hobbs A.J., Kling M. R., Liu Q., Madge D. J., Meillerais S., Powell K. L., Reynolds K., Spacey G. D., Stables J. N., Tatlock M. A., Wheeler K. A., Wishart G., Woo C.K., *J. Med. Chem.* 44 (2001) 78.
18. Lee F.Y., Lien J.C., Huang L.J., Huang T.M., Tsai S.C., Teng C.M., Wu C.C., Cheng F.C., Kuo S.C., *J. Med. Chem.* 44 (2001) 3746.
19. Zhang H.C., Derian C. K., Andrade Gordon P., Hoekstra W. J., Mc Comsey D. F., White K. B., Poulter B. L. Addo M. F., Cheung W.M., Damiano B.P., Oksenberg D., Reynolds E. E., Pandey A., Scarborough R. M., Maryanoff B. E., *J. Med. Chem.* 44 (2001) 1021.
20. Boehm H.J., Boehringer M., Bur D., Gmuender H., Huber W., Klaus W., Kostrewa D., Kuehne 7., Luebbers T. Meunier-Keller N., Mueller F., *J. Med. Chem.* 43 (2000) 2664.
21. Batt D.G., Petraitis J.J., Houghton G.C., Modi D.P., Cain G.A., Corjay M.H., Mousa S.A., Bouchard P.J., Forsythe M.S., Harlow P.P., Barbera F.A., Spitz S.M., Wexler R.R., Jadhav P.K., *J. Med. Chem.* 43 (2000) 41
22. Li X., Chu S., Feher V.A., Khalili M., Nie Z., Margosiak S., Nikulin V., Levin J., Sprankle K. G., Fedder M. E., Almasy R., Appelt K., Yager K. M., *J. Med. Chem.* 46 (2003) 5663.
23. Giragossian C., Sugg E. E., Szewczyk J. R., Mierke D. F., *J. Med. Chem.* 46 (2003) 3476.
24. Wroblewski S. T., Chen P., Hynes J., Lin S., Norris D. J., Pandit C. R., Spergel S., Wu H., Tokarski J. S., Chen X., Gillooly K.M., Kiener P. A., Mc-Intyre K. W., Patil-koota V., Shuster D. J., Turk L. A., Yang G., Leftheris K., *J. Med. Chem.* 46 (2003) 2110.
25. Danaee I., Gholami M., RashvandAvei M., Maddahy M.H., *J. Ind. Eng. Chem.* 26 (2015) 81.
26. Jafari H., Danaee I., Eskandari H., RashvandAvei M., *J. Environ. Sci. Health., Part A* 48 (2013) 1628.
27. Pearson R.G., *Inorg. Chem.* 27 (1988) 734.
28. Sastri V.S., Perumareddi J.R., *Corrosion.* 53 (1997) 617.
29. Elmsellem H., Nacer H., Halaimia F., Aouniti A., Lakehal I., Chetouani A., Al-Deyab S. S., Warad I., Touzani R., Hammouti B., *Int. J. Electrochem. Sci.* 9(2014)5328.
30. Udhayakala P., Rajendiran T. V., Gunasekaran S., *Journal of Chemical, Biological and Physical Sciences A*, 2(3) (2012)1151-1165.
31. Ellouz M., Elmsellem H., Sebbar N. K., Steli H., Al Mamari K., Nadeem A., Ouzidan Y., Essassi E. M., AbdelRahaman I., Hristov P., *J. Mater. Environ. Sci.* 7(7) (2016) 2482-2497.
32. Elmsellem H., Youssouf M. H., Aouniti A., Ben Hadd T., Chetouani A., Hammouti B., *Russian, Journal of Applied Chemistry.* 87(6) (2014) 744-753.
33. Fouda A.S., Shalabi S.K., Elewady G.Y., Merayyed H.F., *Int. J. Electrochem. Sci.* 9 (2014) 7038-7058.
34. Sebbar N. K., Elmsellem H., Boudalia M., lahmidi S., Belleaouchou A., Guenbour A., Essassi E. M., Steli H., Aouniti A., *J. Mater. Environ. Sci.* 6 (11) (2015) 3034-3044.
35. Bouzian Y., Elyoussfi A., Dafali A., Bouhfid R., Elmsellem H., Abdelahi M. M., Nadeem A., Zarrouk A., Essaghoulani A. L., Essassi E. M., *Der Pharmacia Lettre*, 8 (4) (2016) 289-298
36. Chakib I., Elmsellem H., Sebbar N. K., Lahmidi S., Nadeem A., Essassi E. M., Ouzidan Y., Abdel-Rahman I., Bentiss F., Hammouti B., *J. Mater. Environ. Sci.* 7(6) (2016) 1866-1881.
37. Lahmidi S., Elmsellem H., Elyoussfi A., Sebbar N. K., Essassi E.M., Ouzidan Y., Kandri Rodi Y., DguiguiK., El Mahi B. and Hammouti B., *Der Pharma Chemica.* 8(1) (2016) 294.

38. Hjouji M. Y., Djedid M., Elmsellem H., Kandri Rodi Y., Ouzidan Y., Ouazzani Chahdi F., Sebbar N. K., Essassi E. M., Abdel-Rahman I., Hammouti B., *J. Mater. Environ. Sci.* 7(4) (2016) 1425-1435.
39. Filali Baba Y., Elmsellem H., Kandri Rodi Y., Steli H., AD C., Ouzidan Y., Ouazzani Chahdi F., Sebbar N. K., Essassi E. M., Hammouti B., *Der Pharma.Chemica.* 8(4) (2016) 159-169.
40. Hjouji M. Y., Djedid M., Elmsellem H., Kandri Rodi Y., Benalia M., Steli H., Ouzidan Y., Ouazzani Chahdi F., Essassi E. M., Hammouti B., *Der Pharma Chemica.* 8(4) (2016) 85-95.
41. Elmsellem H., Elyoussfi A., Sebbar N. K., Dafali A., Cherrak K., Steli H., Essassi E. M., Aouniti A. and Hammouti B., *Maghr. J. Pure & Appl. Sci.* 1 (2015) 1-10.
42. Elmsellem H., Aouniti A., Khoutoul M., Chetouani A., Hammouti B., Benchat N., Touzani R. and Elazzouzi M., *J. Chem. Pharm. Res.* 6 (2014) 1216.
43. Govindarajan M., Karabacak M., *Spectrochim. Acta Part A Mol Biomol Spectrosc.* 85 (2012) 251.
44. Elmsellem H., Karrouchi K., Aouniti A., Hammouti B., Radi S., Taoufik J., Ansar M., Dahmani M., Steli H., El Mahi B., *Der Pharma Chemica.* 7(10) (2015) 237.
45. Lukovits I., Kalman E., Zucchi F., *Corrosion.* 57 (2001) 3.
46. Elyoussfi A., Dafali A., Elmsellem H., Steli H., Bouzian Y., Cherrak K., El Ouadi Y., Zarrouk A., Hammouti B., *J. Mater. Environ. Sci.* 7 (9) (2016) 3344.
47. Ramdani M., Elmsellem H., Elkhiaati N., Haloui B., Aouniti A., Ramdani M., Ghazi Z., Chetouani A. and Hammouti B., *Der pharma chem.* 7 (2015) 67-76.
48. Sikine M., Elmsellem H., Kandri Rodi Y., Steli H., Aouniti A., Hammouti B., Ouzidan Y., Ouazzani Chahdi F., Bourass M., Essassi E.M., *J. Mater. Environ. Sci.* 7 (12) (2016) 4620-4632.
49. Becke A.D., *Phys. Rev. A.* 38 (1988) 3098.
50. Quijano M.A., Pardav M.P., Cuán A., Romo M.R., Silva G.N., Bustamante R.Á., López A.R., Hernández H.H., *Int. J. Electrochem. Sci.*, 6 (2011) 3729.
51. Kumar S., Ladha D. G., Jha P. C., and Shah N. K., *International Journal of Corrosion* Volume (2013), ID 819643, 10 <http://dx.doi.org/10.1155/2013/819643>.
52. Khaled K. F., *Applied Surface Science*, 256(22)(2010) 6753.
53. Elmsellem H., Elyoussfi A., Steli H., Sebbar N. K., Essassi E. M., Dahmani M., El Ouadi Y., Aouniti A., El Mahi B., Hammouti B., *Der Pharma Chemica.* 8(1)(2016) 248.
54. Lee C., Yang W., Parr R.G., *Phys. Rev. B.* 37 (1988) 785.

(2017) ; <http://www.jmaterenvironsci.com/>